ISSN 1392–1207. MECHANIKA. 2022 Volume 28(5): 351–357

Experimental and Numerical Study on LCF Crack Propagation of Coiled Tubing Steel

Jijia ZHONG*,, Guanghui ZHAO*,***, Qingfeng JIANG****, Litong WANG*, Yi HE*, Sihai HU***

**School of Mechanical Engineering, Southwest Petroleum University, 610500 Chengdu, China,*
E-mails: zhongjichn@163.com; zhaogh@swpu.edu.cn (Corresponding author);202022000840@stu.swpu.edu.cn; 202021000353@stu.swpu.edu.cn; 202122000386@stu.swpu.edu.cn
***Sichuan Aerospace Zhongtian Power Equipment Co. Ltd, 610199 Chengdu, China*
****Oil and Gas Equipment Technology Sharing and Service Platform of Sichuan Province, 610500 Chengdu, China*
*****Sichuan Baoshi Machinery Special Vehicle Co. Ltd, 618300 Deyang, China, E-mail: jiangqf_bs@163.com*

crossref http://dx.doi.org/10.5755/j02.mech.31056

Nomenclature

a – crack dimension, mm; a_0, a_f, a_m – initial crack length, pre-crack length and machined notch length, respectively, mm; C, m – material constants; D – outer diameter, mm; E – Young's modulus, GPa; F – tensile load, kN; f – Frequency, Hz; J, J_0 – J-integral and characteristic J-integral of the crack front, MPa·mm; N – cycle number, cyc; q – load line displacement, mm; R – stress ratio; S – average stress, MPa; t – wall thickness, mm; W – width of the middle test section of the specimen, mm; δ – opening displacement of the notch mouth, mm; σ_y – yield strength, MPa.
Subscript
max – the maximal value; *min* – the minimal value.
Prefix
Δ – increment.

1. Introduction

Coiled tubing (CT) is a thin-walled steel pipe with a diameter of 19.05 - 114.3 mm, a thickness of 1.7018 - 6.096 mm and a length of thousands of meters [1-2]. As there is no need of pipe connection, CT operation shortens working period greatly, reduces field working strength and production cost [3-4]. During one trip, the CT undergoes 3 bending and 3 straightening, and the plastic strain reaches about 2% - 3% [5]. Subjected to both serious plastic deformation and harsh working environment, the tubing usually fails after 100 trips approximately [6-12]. Low-cycle fatigue (LCF) becomes the main factors responsible for the bearing capacity of the CT. With the continuous expansion of CT services, it is increasingly important to reveal the LCF mechanism of the defective CT and predict the remaining life accurately.

For now, LCF performances of the CT are studied mainly through experiments to obtain an empirical or semi-empirical formula. In this field, Avakov et al. [13] conducted pioneering work. Full-scale CTs of several strength levels were tested under tension, internal pressure and alternating bending. LCF life of the CT was forecasted by means of S-N formula, which has been adopted in the engineering software of Halliburton. Tipton carried out extensive research in elastic-plastic properties and LCF failure mechanism of the CT, and proposed fatigue life model that has been used in NOV's drilling & completion software of Cerberus™ and Schlumberger's tubing life prediction software of CoilLIFE™ [14]. Later, Tipton et al. [15] studied the failure theory of multi-axial LCF of CTs experimentally. Based on the Miner linear accumulation theory, the fatigue life prediction model of CTs was established. It was found that the predicted results were reasonable under small internal pressure. Nevertheless, it was difficult for the model to explain the damage caused by circumferential stress along with the increase of internal pressure. For the bending-straightening fatigue tests of CTs, Christian [16] described the strain increase caused by both internal pressure and local defects with "pressure concentration factor" and "strain concentration factor", and proposed a "local strain method" to predict the fatigue life of CTs. Ryu et al. [17] determined parameters of various cyclic hardening models for the CT through LCF tests, and found that the kinematic and combined hardening models could all be used in predicting the fatigue life of CTs, but the results were conservative relatively. Liu et al. [18] studied the effect of internal pressure on the fatigue life of CTs based on the elastic-plastic theory and LCF experiments, and indicated that internal pressure was one of the major factors affecting the bearing capacity of CTs. These studies were all about perfect CTs, and presented empirical formulas or variation tendencies through experiments or theoretical analysis [19]. The crack propagation law during cyclic loading was not researched, and effects of different loading conditions on the fatigue failure of CTs cannot be distinguished one from another.

At present, there are very few studies on fatigue and fracture properties of the cracked CT. Effects of various surface defects on fatigue life of CTs had been analyzed statistically by Christian and Tipton [20] and Padron et al. [21], which showed that the defect whose depth was between 2% and 42% of the wall thickness could reduce the fatigue life by 48% to 75%. Wainstein and Ipina [6-7] machined a 1-m-long CT with a circumferential through-wall crack and carried out four-point bending tests to determine J-R curves. In order to simplify the test process, they used S_{pb} (separability parameter) to measure crack lengths and J-R curves, and obtained satisfied results [8]. Up to now, the crack propagation law of a defective CT under fatigue load has not been reported.

The most common method for describing the growth rate of a high-cycle fatigue crack is the Paris' law. But it does not work for LCF crack because a large plastic zone exists near the crack tip. Instead, J-integral should be

used as the main parameter to describe crack growth rates of the LCF, which is expressed as:

$$\frac{\mathrm{d}a}{\mathrm{d}N} = C \cdot (\Delta J)^m , \quad (1)$$

where: a is the crack dimension; N is the cycle number; C and m are material constants; $\Delta J = J_{max} - J_{min}$, J_{max} and J_{min} are the J-integrals corresponding to the maximal load F_{max} and the minimal load F_{min}, respectively. Using Eq. (1), the residual fatigue life of the CT can be predicted under a given cyclic load if C and m are known.

This paper aims to determine the material constants of C and m to describe the LCF crack growth rates of the CT steel. Firstly, single-edge-notched (SEN) arc specimens were machined, and crack growth rates of specimens with different crack lengths were measured under cyclic tension. Secondly, finite element (FE) simulation was conducted to discover the relationship among J-integral, load and crack dimension. Finally, taking test results and FE results together, an explicit expression of ΔJ is given to describe the LCF crack growth rates da/dN, which is essential for predicting the service life of the CT with method of fracture mechanics.

2. LCF crack growth tests with force-controlled mode

2.1. Specimens and experimental setup

The CT used in the test was taken from the oil field. It was the same batch as the tubing used in Ref. [21]. The CT was of outer diameter D = 38.1 mm, wall thickness t = 3.18 mm, and the true stress-true strain curve was shown in Fig. 1. The Young's modulus is E = 206 GPa and the yield strength is σ_y = 494 MPa.

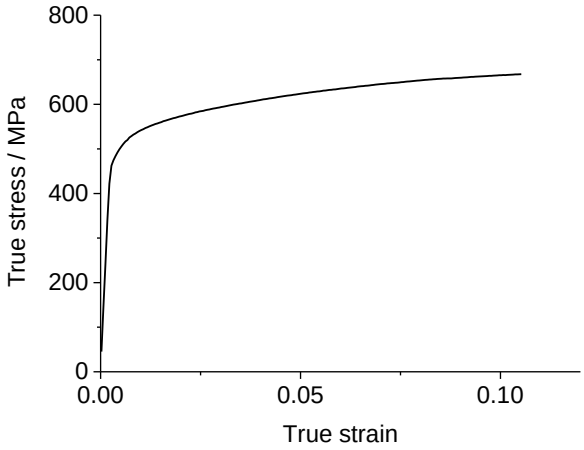

Fig. 1 True stress-true strain curve of CT steel [22]

Because of small diameter and thin wall, it is difficult to make standard fracture specimens. In order to avoid effects of both thickness and curvature on the test results, specimens were taken directly from the CT axially, and kept the same arc shape as the CT, as shown in Fig. 2 [22-23]. The width of the middle test section was W = 17 mm. A notch was machined on one side in the middle section. The clamping section is also kept curved with a length of 43 mm. Special grip inserts, designed as Fig. 3 were machined to hold the specimens, and ensure the tensile load passing through the centroid of the test section of the specimen.

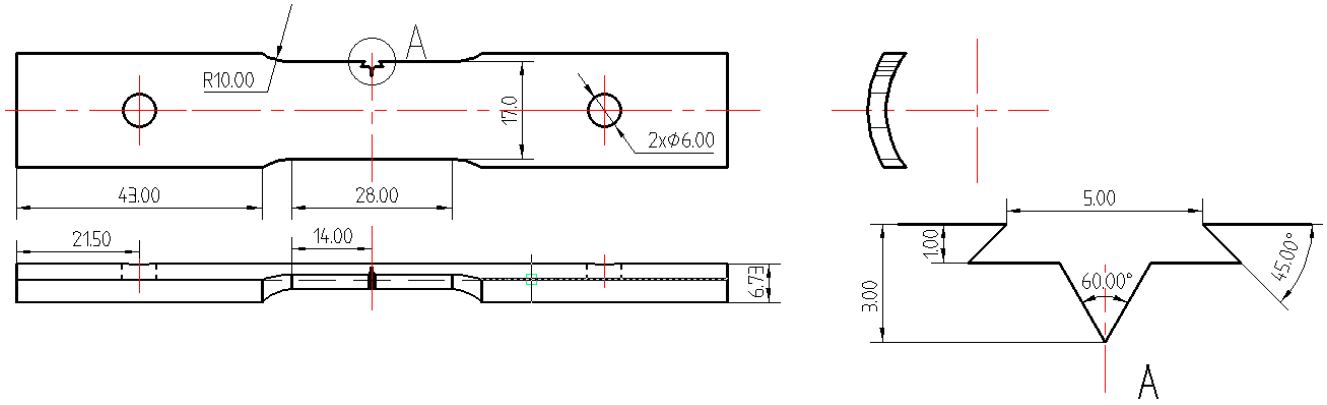

Fig. 2 Dimension of the SEN arc specimen (mm)

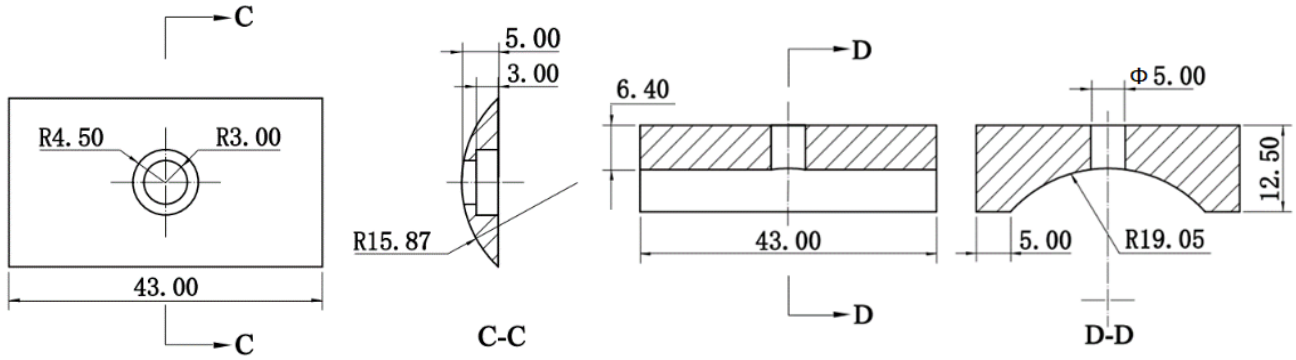

a b

Fig. 3 Dimensions of grip inserts (unit: mm): a) internal intert; b) external insert

The LCF crack growth test was conducted on an MTS machine, as shown in Fig. 4. The load line displacement q and tensile load F were measured by the built-in sensors of the MTS [24-25]. The crack mouth opening displacement (CMOD) of the notch mouth, denoted as δ, was measured by a COD gauge, and the crack propagating process was recorded by a CCD camera.

First of all, sharp fatigue cracks were pre-fabricated for all specimens. Force-controlled loading mode, with sinusoidal shape, was adopted. The average and amplitude of the force were 4.25 kN and 3.75 kN, respectively, and the loading frequency was 10 Hz. The pre-crack front of the arc specimen was a curve, as shown in Fig. 5. The crack length was defined as arc length along the mid-line at 1/2 wall thickness of the specimen. The initial crack length a_0 consisted of two parts: the machined notch length a_m and the pre-crack length a_f, i.e., $a_0 = a_m + a_f$.

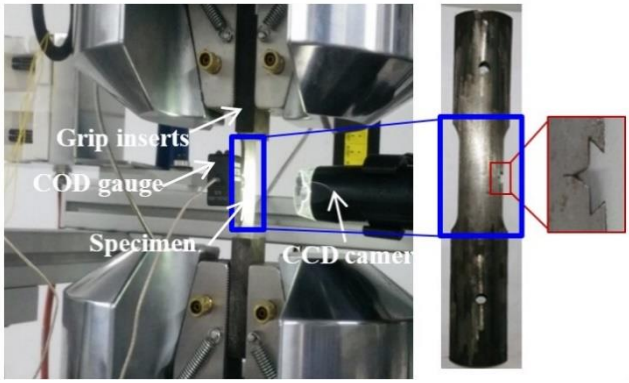

Fig. 4 LCF test of the SEN arc specimen on an MTS machine

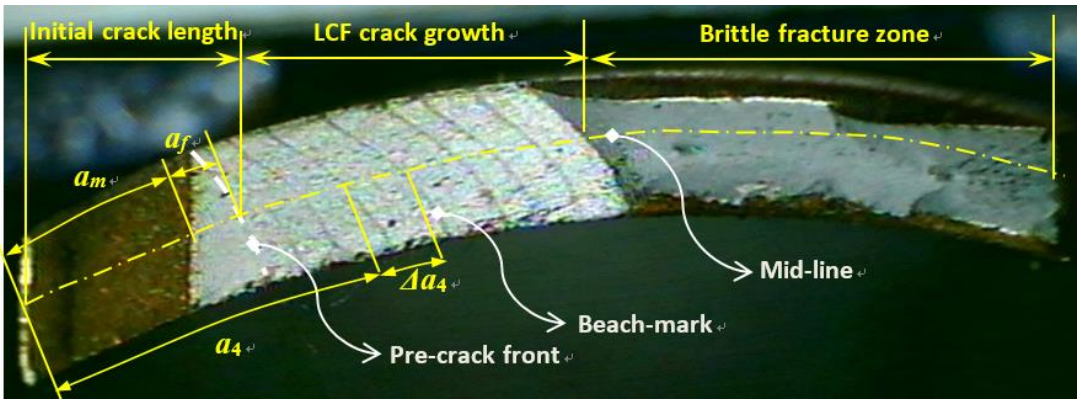

Fig. 5 Fracture surface of the broken arc specimen CF4

2.2. Loading conditions and process

LCF tests were conducted also with sinusoidal force-controlled mode. The maximal force F_{max} of the LCF test should be large enough to make the specimen deforming plastically near the crack front, and was determined by monotonic tensile tests. Therefore, three pre-cracked arc specimens were pulled monotonically firstly. These 3 specimens were denoted as MT1, MT2 and MT3, whose initial crack lengths were a_0 = 3.56 mm, 3.79 mm and 4.05 mm, respectively. The relationships between F and q were obtained as shown in Fig. 6. It shows that F-q curves gradually deviate from linearity when F is larger than 11 kN. It means that a large range of plastic deformation happened to the specimens. Therefore, the F_{max} of the LCF test was taken as 11 kN. The stress ratio R was chosen as 0.1 to avoid reverse loading, and the loading frequency f was 3 Hz. Notice that the numerical result drawn as dashed line in Fig. 6 will be used in Section 3.1.

In the process of the LCF test, *Crack Front Marking Technique* was used to generate beach-marks on the fracture surface and figure out the crack propagation length. The test procedure is described as follows. In the first LCF process, the specimen with a certain initial crack length a_0 was loaded cyclically (F_{max} = 11 kN, R = 0.1 and f = 3 Hz) until the estimated crack growth length reached about 1 mm. Then *Crack Front Marking* process began. Keeping the average load the same, the loading amplitude was reduced by half and the frequency was increased to 10 Hz. As the crack grew about 0.1 mm, which looked like a piece of darker beach-mark on the fracture surface as shown in Fig. 5, the *Marking* process was completed. Then using the beach-mark as the new initial crack front and increasing the F_{max} again to 11 kN, the second LCF process began and so on.

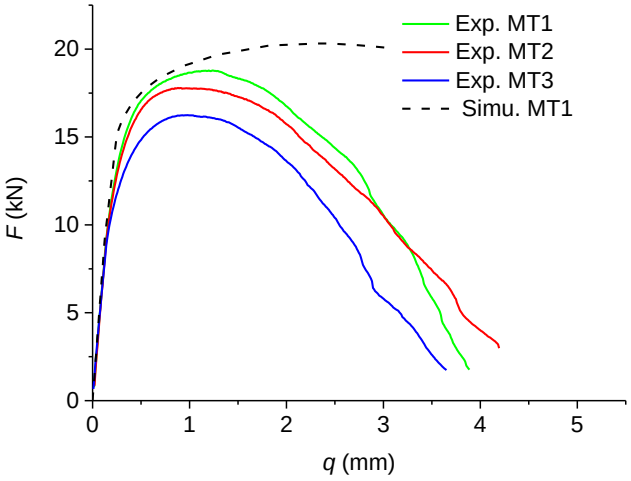

Fig. 6 F-q curve of monotonic tensile tests

The testing process went on until the specimen was broken. Fig. 5 shows a fracture surface of one specimen, which had undergone 8 LCF processes and 7 *Crack Front Marking* processes. The space between adjacent beach-marks is the crack propagation length Δa of each LCF process. Taking the 4th LCF process as an example, Fig. 5 indicates the initial crack length a_4 and the crack propagation length Δa_4. Thus, the crack growth rate da/dN can be obtained through the ratio of Δa to the corresponding cycle number ΔN.

2.3. LCF test results

LCF tests were conducted with 4 specimens. These specimens, denoted as CF1, CF2, CF3 and CF4, were subjected to 6, 3, 4 and 8 LCF cycles, respectively. Fig. 5 is the fracture surface of the broken arc specimen CF4. Corresponding to each LCF cycle, test parameters including the initial crack length a, cycle number ΔN and crack propagation length Δa are given in Table 1, and time histories of both δ and q were recorded. Taking CF3 as an example, the 1st to 4th LCF processes are illustrated in Fig. 7a - d, respectively. In each sub-image of Fig. 7, variations of parameters, including the maximal value and minimal value of both load line displacement and CMOD increment (q_{max}, q_{min}, $\Delta\delta_{max}$ and $\Delta\delta_{min}$), with cycle number N are presented. Here CMOD increment, denoted as $\Delta\delta$, is the difference of the real-time CMOD and the initial CMOD. It is found that the extreme value of both q and the $\Delta\delta$ all increase gradually as the cycle number N increases. It infers that cyclic softening had happened to the specimen. This phenomenon is attributed to crack extension and cycle deterioration of the material itself.

Table 1 also presents the crack growth rate da/dN, which increases gradually along with the crack length increasing. From Table 1, relationship among da/dN, a and ΔF (= F_{max} - F_{min}) could be developed. To determine material constants of C and m of Eq. (1), in which da/dN is expressed by J-integral, function of J-F-a are also needed. For the non-standard SEN arc specimen of the present work, this function would be obtained by means of FE simulation.

Table 1

Parameters and results of LCF tests (F_{max} = 11 kN, R = 0.1)

Specimen	No. of times	a, mm	ΔN, cyc	Δa, mm	da/dN, 10^{-3} mm/cyc
CF1	1	3.914	899	0.425	0.473
	2	4.339	894	0.562	0.629
	3	4.902	894	0.709	0.793
	4	5.611	892	1.051	1.18
	5	6.662	901	1.115	1.24
	6	7.777	898	1.121	1.25
CF2	1	5.26	1942	1.203	0.62
	2	7.07	1197	1.719	1.44
	3	8.535	698	1.194	1.71
CF3	1	4.806	899	0.510	0.568
	2	5.535	898	0.609	0.678
	3	6.354	798	0.733	0.919
	4	7.118	500	0.657	1.31
CF4	1	3.808	1999	0.417	2.09
	2	4.241	1798	0.463	2.58
	3	4.733	1997	0.551	2.76
	4	5.344	2201	0.777	3.53
	5	6.152	1798	0.827	4.60
	6	7.039	800	0.420	5.25
	7	7.519	999	0.650	6.51
	8	8.229	998	0.741	7.43

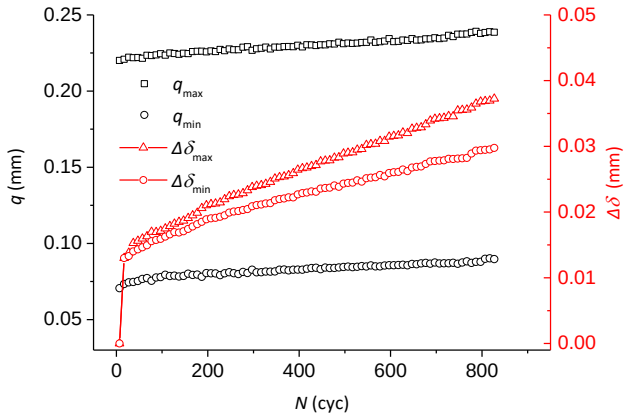

a

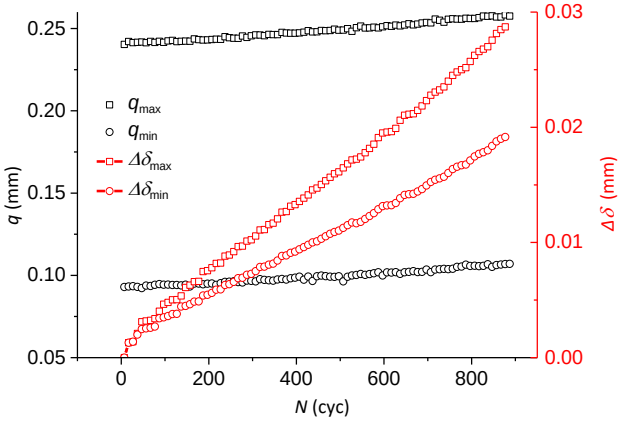

b

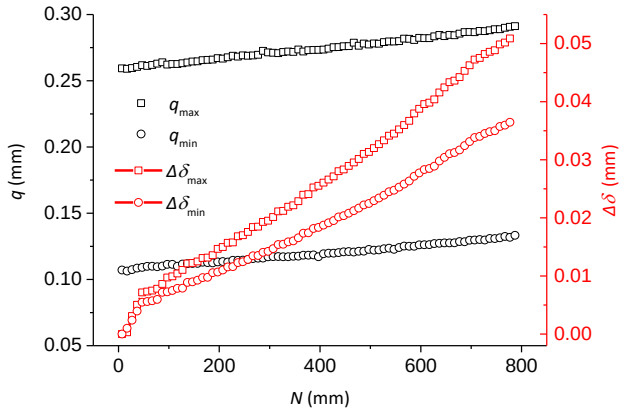

c

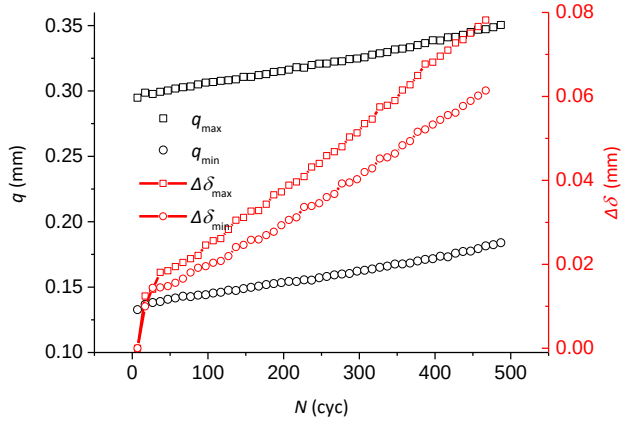

d

Fig. 7 Variatins of the extreme values of q and $\Delta\delta$ with N for CF3: a) the 1st LCF process; b) the 2nd LCF process; c) the 3rd LCF process; d) the 4th LCF process

3. FE analysis of ductile fracture properties

FE software ABAQUS will be used to simulate the static ductile fracture properties of the present SEN arc specimen, and get the function of *J*-*F*-*a*. To be noted, crack growth is not included in the FE analysis.

3.1. FE model and validation

According to dimensions of the arc specimen (see Fig. 2), FE models with crack lengths varying from 3mm to 9mm are developed. This range of crack length covers the initial crack lengths listed in Table 1. As an example, the FE model with the crack length a = 4 mm is presented in Fig. 8(a). For simplicity, both the machined notch and the prefabricated fatigue crack are modelled with one crack plane. The material property is defined with the true stress-true strain relationship presented in Fig. 1. One end of the model is fixed, and the other end is applied with a distributed force F in the axial direction. The model is meshed with 8-node hexahedral solid elements (C3D8R), and divided into 8 parts along the thickness direction. In-plane mesh is refined near the crack front. The *refinement zone* is a circle with a radius of 2 mm, as shown in Fig. 8b. The 1/4 circumference and radius of the *refinement zone* are all equally divided into 10 parts, while the in-plane dimension of the rest zone of the test section is 0.5 mm. The maximum mesh size of the model is 1 mm. The model has a total of 75,114 nodes and 65,112 units. The *J*-integral of a crack tip is calculated by the contour integral in the plane normal to the crack front. 10 contour integrals are extracted around the crack tip, and the average of the 4th to 8th contour integrals is taken as the *J*-integral of the tip.

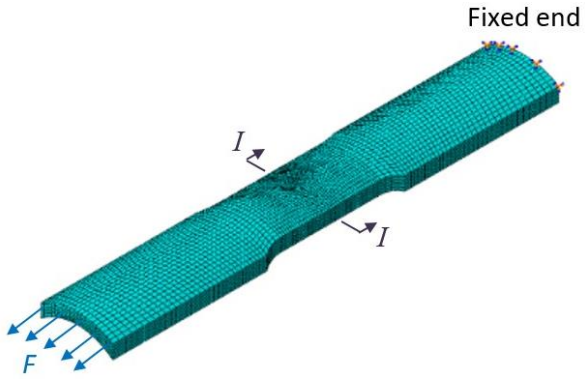

a

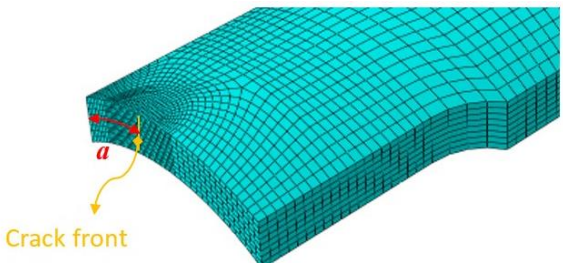

b

Fig. 8 The FE model of the CT specimen: a) the whole model; b) enlarged view of meshes near the crack front from cross section *I*-*I*

To validate the FE method, the FE model of the specimen MT1 (a_0 = 3.56 mm) is established, and the relationship between F and q is calculated and presented by a dashed line in Fig. 6. Compared with the measured F-q curve of MT1, the numerical result is almost the same for the linear stage and the most ascent stage of the experimental result, and the relative error is only 1.9% for q = 0.7 mm. For larger q, difference between these two curves increases sharply. That means the crack is growing. As a result, the predicted result is consistent with the tested result before the crack grows, and the correctness of the FE method could be validated. So, the FE model established in this section will be used to build relationships of *J*-*F*-*a*.

3.2. Ductile fracture properties

For simplicity, the *J*-integral at the 1/2 wall thickness is specified as characteristic *J*-integral of the crack front, and denoted as J_0. For specimens with different crack size a, variation of J_0 with load F is calculated. To avoid the influence of the machining error on the results, the average stress S is defined on the initial ligament of the specimen as: $S = F/\left[(W-a)\times t\right]$. J_0-S curves for specimens with different a were obtained and presented in Fig. 9. It shows that *J*-integrals increase along with F increasing for a certain crack size. And the larger the crack size is, the larger the slope of the J_0-S curve is. That means a larger growth rate of *J*-integral with load. For a certain load S, the *J*-integral increases rapidly as the crack grows. Based on the predicted relationships of J_0-S-a and the test results in Section 2, material constants of C and m in the Eq. (1) can be determined.

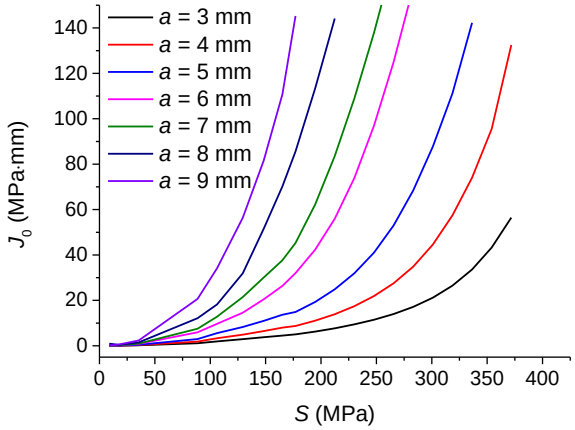

Fig. 9 J_0-S curves for different crack size a

4. LCF crack growth rate

Using the relationship of J_0-S-a given in Fig. 9, the *J*-integral corresponding to two parameters of a and F, which are listed in Table 1, could be determined by means of linear interpolation method. J_{max} and J_{min} are connected to F_{max} and F_{min}, respectively, and $\Delta J = J_{max} - J_{min}$. The d$a$/d$N$ and the corresponding ΔJ are plotted in a logarithmic coordinate system as shown in Fig. 10. Then, an exponential function is fitted according to Eq. (1), and the material constants could be determined as: C = 3.784 × 10^{-6} and m = 1.126. That is to say, the explicit expression of the crack growth rate of the present CT steel is:

$$\frac{\mathrm{d}a}{\mathrm{d}N} = 3.784\times10^{-6}\cdot\left(\Delta J\right)^{1.126}. \quad (2)$$

Using Eq. (2), the LCF life of the CT can be predicted when the *J*-integrals corresponding to the maximal and minimal loads during the CT operation are known.

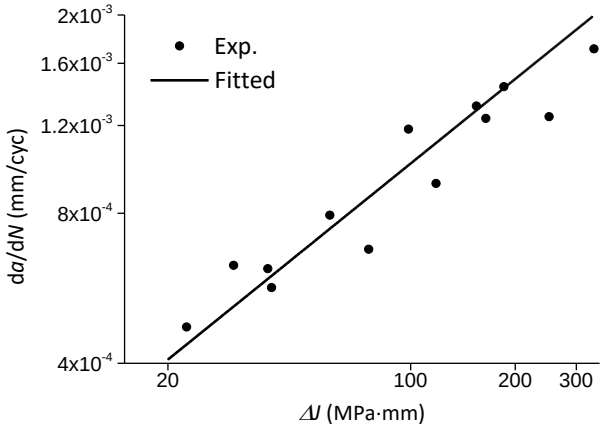

Fig. 10 Relationship between d*a*/d*N* and Δ*J*

5. Conclusions

1. For the characteristics of thin wall and small diameter of CT, SEN arc specimens of a CT were designed and machined. The LCF tests with force-controlled mode were conducted and the crack growing processes were measured. Cyclic softening property of the CT steel was presented through time histories of extreme values of both CMOD increment and load line displacement.

2. The crack growth length was measured by means of *Crack Front Marking Technique*, and the relationship between the crack propagating rate and the crack length is obtained under the force-controlled loading condition.

3. The FE model of the SEN arc specimen is established and validated. Relationships among the characteristic *J*-integral, crack size and load are obtained by the FE calculation.

4. Based on the crack growth rate d*a*/d*N* measured from the LCF tests and the *J*-integral predicted by the FE method, the d*a*/d*N* is expressed as an explicit function of *ΔJ* for the present CT steel. It is essential for predicting the LCF life of CT under working conditions by means of method of fracture mechanics.

Acknowledgment

This project was supported by the Open Fund of Key Laboratory of Oil & Gas Equipment, Ministry of Education (SWPU).

References

1. **Liu, Z. K.; Zheng, A.; Oscar, O. R. D.; Lauren, H.** 2015. A novel fatigue assessment of CT with defects based on magnetic flux leakage, SPE-173664-MS. https://doi.org/10.2118/173664-MS.
2. **Liu, S. H.; Guan, F.; Wu, X. J.; Xiao, H.; Wang, Z.; Yang, T. G.** 2019. Theoretical and experimental research of bearing capacity and fatigue life for coiled tubing under internal pressure, Engineering Failure Analysis 104: 1133-1142. https://doi.org/10.1016/j.engfailanal.2019.06.062.
3. **Ghobadi, M.; Muzychka, Y. S.** 2014. Pressure drop in mini-scale coiled tubing, Experimental Thermal and Fluid Science 57 (3): 57-64. https://doi.org/10.1016/j.expthermflusci.2014.04.011.
4. **Guan, F.; Miao, Z. P.; Zhou, C. X.; Xu, J.; Wan, F.; Liu, S. H.; Yang, T.; Wu, J. W.** 2017. Development on coiled tubing fracturing sleeve for shale gas horizontal well, Advances in Mechanical Engineering 9(5): 1-9. https://doi.org/10.1177/1687814017705063.
5. **Tipton, S. M.** 1998. Low cycle fatigue testing of tubular material using non-standard specimens, Effects of Product Quality and Design Criteria on Structural Integrity, St. Louis, MO, USA, p. 102-119
6. **Wainstein, J.; Ipiña, J. P.** 2012. Fracture toughness of HSLA coiled tubing used in oil wells operations, Journal of Pressure Vessel Technology 134 (1): 011403. https://doi.org/10.1115/1.4004569.
7. **Wainstein, J.; Ipiña, J. P.** 2012. Ductile instability analysis of HSLA coiled tubing, Procedia Materials Science 1: 297-304. https://doi.org/10.1016/j.mspro.2012.06.040.
8. **Wainstein, J.; Ipiña; J. P.** 2017. The S_{pb} method used to estimate crack extension for coiled tubings fracture toughness tests, Engineering Fracture Mechanics 178: 362-374. https://doi.org/10.1016/j.engfracmech.2017.03.014.
9. **Liu, S. H.; Xiao, H.; Guan, F.; Jiang, Q. F.; Wu, J. W.; Yang, T.** 2017. Coiled tubing failure analysis and ultimate bearing capacity under multi-group load, Engineering Failure Analysis 79: 803-811. https://doi.org/10.1016/J.Engfailanal.2017.05.007.
10. **Hampson, R.; Eric, J.; Tyler, S.** 2016. Predicting coiled tubing life should consider diameter growth in addition to low-cycle fatigue, SPE-179078-MS. https://doi.org/10.2118/179078-MS.
11. **Padron, T.; Craig, S. H.** 2018. Past and present coiled tubing string failures-history and recent new failures mechanisms, SPE-189914-MS. https://doi.org/10.2118/189914-MS.
12. **Zhao, G. H.; Li, J.; Zhang, Y. X.; Liang, Z; Yang C. H.** 2018. An inverse analysis-based optimal selection of cohesive zone model for metallic materials, International Journal of Applied Mechanics 10(2): 1850015. https://doi.org/10.1142/S1758825118500151.
13. **Avakov, V. A.; Foster, J. C.; Smith, E. J.** 1993. Coiled tubing life prediction, Offshore Technology Conference Report No. OTC-7325-MS. https://doi.org/10.4043/7325-MS.
14. **Tipton, S. M.; Newburn, D. A.** 1990. Plasticity and fatigue damage modeling of severely loaded tubing, Proc. Conf. Advances in Fatigue Lifetime Predictive Techniques, San Francisco, California, USA, p. 369-382. https://doi.org/10.1016/0142-1123(93)90113-5.
15. **Tipton, S. M.; Neuharth, L. G.; Sorem, J. R.** 2006. Influence of prior cycling on fatigue damage caused by defects in coiled tubing, SPE-100199-MS. https://doi.org/10.2118/100199-MS.
16. **Christian, A.** 2010. Local strain approach for fatigue life prediction of coiled tubing with surface defects, Ph.D. Thesis, University of Tulsa, Oklahoma, USA.
17. **Ryu, T. Y.; Choi, J. B.; Huh, N. S.; Kang, S. C.; Kim, K. S.** 2018. Effects of work hardening models on low-cycle fatigue evaluations of coiled tubing with CT-100 steel, Journal of Mechanical Science and Technology 32 (11): 5055-5061. https://doi.org/10.1007/S12206-018-1001-3.

18. **Liu, S. H; Guan, F.; Wu, X. J.; Xiao, H.; Wang, Z; Yang, T. G.** 2019. Theoretical and experimental research of bearing capacity and fatigue life for coiled tubing under internal pressure, Engineering Failure Analysis 104: 1133-1142. https://doi.org/ 10.1016/j.engfailanal.2019.06.062.
19. **Spagnol, J.; Wu, H.; Yang, C. H.** 2020. Application of non-symmetric bending principles on modelling fatigue crack behaviour and vibration of a cracked rotor, Applied Sciences 10(717): 1-29. https://doi.org/10.3390/app10020717.
20. **Christian, A.; Tipton, S. M.** 2009. Statistical analysis of coiled tubing fatigue data, SPE-121457-MS. https://doi.org/10.2118/121457-MS.
21. **Padron, T.; Luft, B.; Kee, E.; Tipton, S. M.** 2007. Fatigue life of coiled tubing with external mechanical damage, SPE-107113-MS. https://doi.org/10.2118/107113-MS.
22. **Zhao, G. H.; Li, J.; Zhang, Y. X.; Zhong, J. J.; Liang, Z.; Xiao, S. H.** 2019. A study on ductile fracture of coiled tubing based on cohesive zone mode, Engineering Fracture Mechanics 209: 260-273. https://doi.org/10.1016/j.engfracmech.
23. **Tipton, S. M.** 2000. Coiled tubing surface characteristics and effects on fatigue behavior, SPE Drilling & Completion 15(1): 63-66. https://doi.org/10.2118/62096-PA.
24. **Bazaras, Z.; Cesnavicius, R.; Bazariene, J. I.; Kersys, R.** 2017. Investigation of the probabilistic low cycle fatigue design curves at stress cycling, Mechanika 32(2): 176-181. http://dx.doi.org/10.5755/j01.mech.23.2.14358.
25. **Solomon, I.; Narvydas, E.; Dundulis, G.** 2021. Stress-strain state analysis and fatigue prediction of D16T alloy in the stress concentration zone under combined tension-torsion load, Mechanika 27(5): 368-375. http://dx.doi.org/10.5755/j02.mech.28454.

J. J. Zhong, G. H. Zhao, L. T. Wang, Y. He, S. H. Hu

EXPERIMENTAL AND NUMERICAL STUDY ON LCF CRACK PROPAGATION OF COILED TUBING STEEL

S u m m a r y

Coiled tubing (CT) is a joint-less long oil pipe that is wound around a reel and can be run and pulled continuously. Due to the particularity of the operating process, low-cycle fatigue (LCF) failure of the CT constitutes the main production cost. Aiming at the characteristics of small diameter and thin wall of CT, a single-edge-notched (SEN) arc specimen was designed and machined. LCF tests were conducted with force-controlled mode. Cyclic softening of the CT steel was presented and crack growing rates were measured. Meanwhile, finite element simulation was carried out to obtain the relationships among *J*-integral, crack size and load. Based on the experimental and numerical results, the speed of the LCF crack growth of the CT steel is expressed as an explicit function of the *J*-integral. It provides a basis for predicting the LCF life of the CT under working conditions from the perspective of crack propagation.

Keywords: coiled tubing (CT), low-cycle fatigue (LCF), crack growth rate, experimental study, *J*-integral.

Received April 01, 2022
Accepted October 17, 2022